Traffic 2007; **8:** 486–499
Blackwell Munksgaard

doi: 10.1111/j.1600-0854.2007.00548.x

The Ternary Rab27a–Myrip–Myosin VIIa Complex Regulates Melanosome Motility in the Retinal Pigment Epithelium

Vanda S. Lopes[1], José S. Ramalho[2], Dylan M. Owen[3], Mike O. Karl[4], Olaf Strauss[4], Clare E. Futter[5] and Miguel C. Seabra[1,*]

[1]Molecular and Cellular Medicine, Faculty of Medicine, Imperial College London, London SW7 2AZ, UK
[2]Centre of Ophthalmology, Biomedical Institute for Research in Light and Image, University of Coimbra, 3000-354 Coimbra, Portugal
[3]Chemical Biology Centre, Imperial College London, London, SW7 2AZ, UK
[4]Bereich Experimentelle Ophthalmologie, Klinik und Poliklinik fuer Augenheilkunde, Universitaetsklinikum Hamburg-Eppendorf, 20246, Hamburg, Germany
[5]Division of Cell Biology, Institute of Ophthalmology, University College London, London EC1V 9EL, UK
**Corresponding author: Miguel C. Seabra, m.seabra@imperial.ac.uk*

The retinal pigment epithelium (RPE) contains melanosomes similar to those found in the skin melanocytes, which undergo dramatic light-dependent movements in fish and amphibians. In mammals, those movements are more subtle and appear to be regulated by the Rab27a GTPase and the unconventional myosin, Myosin VIIa (MyoVIIa). Here we address the hypothesis that a recently identified Rab27a- and MyoVIIa-interacting protein, Myrip, promotes the formation of a functional tripartite complex. In heterologous cultured cells, all three proteins co-immunoprecipitated following overexpression. Rab27a and Myrip localize to the peripheral membrane of RPE melanosomes as observed by immunofluorescence and immunoelectron microscopy. Melanosome dynamics were studied using live-cell imaging of mouse RPE primary cultures. Wild-type RPE melanosomes exhibited either stationary or slow movement interrupted by bursts of fast movement, with a peripheral directionality trend. Nocodazole treatment led to melanosome paralysis, suggesting that movement requires microtubule motors. Significant and similar alterations in melanosome dynamics were observed when any one of the three components of the complex was missing, as studied in *ashen*- (Rab27a defective) and *shaker-1* (MyoVIIa mutant)-derived RPE cells, and in wild-type RPE cells transduced with adenovirus carrying specific sequences to knockdown Myrip expression. We observed a significant increase in the number of motile melanosomes, exhibiting more frequent and prolonged bursts of fast movement, and inversion of directionality. Similar alterations were observed upon cytochalasin D treatment, suggesting that the Rab27a–Myrip–MyoVIIa complex regulates tethering of melanosomes onto actin filaments, a process that ensures melanosome movement towards the cell periphery.

Key words: melanosome motility, Myrip, Rab27a, RPE

Received 18 September 2006, revised and accepted for publication 30 January 2007, published online 26 March 2007

The retinal pigment epithelium (RPE) is part of the blood/retina barrier and is composed of a pigmented monolayer of polarized cells performing multiple functions. These include absorption of light and protection against photo-oxidation, transepithelial transport of nutrients, spatial buffering of ions in the subretinal space, cycling of retinal, phagocytosis and secretion of a variety of growth factors (1,2). The apical membrane forms long processes that face and partially envelop the photoreceptor outer segments. This close interaction between RPE and photoreceptors is essential for visual function. The RPE phagocytoses the tips of shed photoreceptor outer segments and is necessary for recycling of retinal used by photoreceptor opsins. On its basolateral side, the RPE faces Bruch's membrane and the fenestrated endothelium of the choriocapillaris.

Melanin pigment is contained within the cytoplasm in melanosomes of skin and choroidal melanocytes, and RPE (1). Pigment must play an important role in the development of the neural retina because albino mice, lacking the key melanogenic enzyme tyrosinase, present abnormal patterns of cell proliferation and reduced numbers of photoreceptors (3). In adults, melanosomes may be important in absorption of stray light and free radicals. Contrary to fish and amphibians where melanosomes of the RPE redistribute dramatically from the cell body into the apical processes upon onset of light in a reversible manner, mammalian melanosomes undergo only a modest light and/or circadian cycle-dependent redistribution into the apical processes (1,4), and exhibit motility in isolated primary RPE cultures (1,5).

The process of melanosome motility has been extensively studied in melanocytes of the skin. Once mature, melanosomes are first transported to the peripheral region of the cell by long-range, bidirectional, microtubule (MT)-dependent movements and are then transferred to actin filaments and carried by short-range, local movements (6,7).

The association with actin serves as a peripheral retention mechanism (8), after which they are translocated from the melanocyte dendrites to adjacent epidermal keratinocytes (9). Translocation from MT-based to actin-based transport requires a tripartite complex, composed of Rab27a, Melanophilin (Mlph) and Myosin Va (MyoVa). Rab27a attached to the melanosome membrane binds Mlph, a linker protein that in turn binds to MyoVa, the actin-based motor (10–12). Loss of any of the partners of the complex leads to clustering of the melanosomes in the perinuclear region, as shown in studies involving melanocytes from *ashen* (lacking functional Rab27a) (13), *leaden* (mutant for Mlph) (14,15) and *dilute* (absence of MyoVa) (8), resulting in coat colour dilution in mice and partial albinism in humans.

The movement along MTs has been extensively studied in melanophores, where pigment aggregation and dispersion can be easily manipulated by addition of melatonin and melanocyte-stimulating hormone, respectively, revealing the role of MTs and their associated motors, dynein and kinesin, in pigment distribution (16). The mechanism by which two motors of opposite polarity act to control the bidirectional movement of melanosomes on MTs originally described by a tug-of-war model (17) was more recently suggested to occur via a MT-motor co-ordination model (18). On the other hand, co-ordination between actin- and MT-based movement appears to be regulated by a tug-of-war mechanism, where both motors are present in the same cargo molecule at the same time (19), and impairment of one component, such as actin in MyoVa-deficient cells, increases the contribution of the other (8,17,20). These studies proposed that MyoVa acts by terminating a minus-end run and moving the melanosome away from the MT network, its action being regulated by the number of MyoVa molecules associated with cargo (17).

Contrary to what is known for melanophores and melanocytes, the contribution of each cytoskeletal filament system in melanosome transport is not well understood in RPE cells. Studies in cultures of dissociated fish RPE cells, which undergo dramatic pigment granule movement as observed in melanophores (16), using the MT-dissociating agent nocodazole suggested that MTs had no effect on aggregation or dispersion of pigment, while the actin-depolymerizing agent cytochalasin D inhibited both dispersion and aggregation, as well as impaired the maintenance of the fully aggregated and dispersed states (21). In mammals, the molecular mechanisms involved in melanosome movement in the RPE are much less well characterized, but recent evidence points to a conserved mechanism with skin melanocytes (11). Rab27a appears to recruit another unconventional myosin, Myosin VIIa (MyoVIIa), for the movement of melanosomes into the apical processes of the RPE. In *ashen* and *shaker-1* (lacking functional MyoVIIa) mice mutant strains, the distribution of RPE melanosomes is altered, with melanosomes found exclusively in the cell body of the RPE, failing to move beyond the level of the adherens junctions (4,5,22). The RPE in *leaden* mice appears normal, indicating that Mlph does not act as the linker protein between Rab27a and MyoVIIa in RPE cells (4,5). A likely candidate for a Rab27a and MyoVIIa linker protein is Myrip [also called synaptotagmin-like protein lacking C2 domains (Slac2-c)]. Myrip is a 96-kDa protein, which was originally identified as a MyoVIIa tail-binding protein (23,24). Myrip contains a typical Rab27a-binding motif, is able to bind to MyoVIIa and Rab27a and is expressed in the RPE where it associates with melanosomes (23). However, the direct involvement of Myrip in melanosome motility in the RPE remains to be demonstrated. This issue represents the focus of the present study.

Results

Formation of a tripartite complex between Rab27a, Myrip and MyoVIIa in the RPE

In order to establish a system to address the hypothesis that Myrip serves as a functional linker between Rab27a and MyoVIIa in RPE, we developed a mouse RPE primary cell culture based on Wollmann et al. (25,26). The RPE cultures were essentially clear of any other retinal cell type, and RPE primary cells maintained their characteristic physiological features, such as cuboidal shape and pigmentation (Figure 1 A). Immunoblot of primary cell extracts showed the expression of the RPE-specific marker RPE65 and Rab27a at comparable levels to skin melanocytes (Figure 1B). We generated a specific antibody against Myrip and detected endogenous Myrip in RPE primary cultures but not in skin melanocytes (Figure 1B). We did not assay for MyoVIIa due to lack of a suitable antibody but its expression in RPE cells has been reported previously (5). We also attempted to detect expression of the melanocyte-specific isoform of MyoVa in the RPE cultures, but the results were negative despite loading twice the amount of protein compared to controls (wild-type melanocytes and HEK-293 cells) (Figure 1B).

In order to test whether Rab27a, Myrip and MyoVIIa could potentially form a complex, we used a heterologous expression system and performed co-immunoprecipitation studies (Figure 1C). COS-7 cells were co-transfected with green fluorescent protein (GFP)-Myrip, untagged Rab27a and V5-MyoVIIa tail [corresponding to amino acids (aa) 1671-stop]. Total extracts were assayed for the presence of the overexpressed proteins, and then incubated with anti-V5 antibody. V5-MyoVIIa tail immunoprecipitates also contained Rab27a and Myrip. Both full-length and a Myrip fragment containing aa 1–414 were able to associate with both Rab27a and MyoVIIa (Figure 1C). In the absence of Rab27a input or when using a deletion Myrip (195–414) construct, MyoVIIa tail was still able to pull-down Myrip, as expected from the proposed model where Myrip serves as a linker protein between Rab27a and MyoVIIa. Conversely, a fragment of Myrip encoding aa 407–652 was unable to co-immunoprecipitate with MyoVIIa tail. Therefore, the fragment 1–414 of Myrip appears necessary and sufficient to establish the link between MyoVIIa and Rab27a.

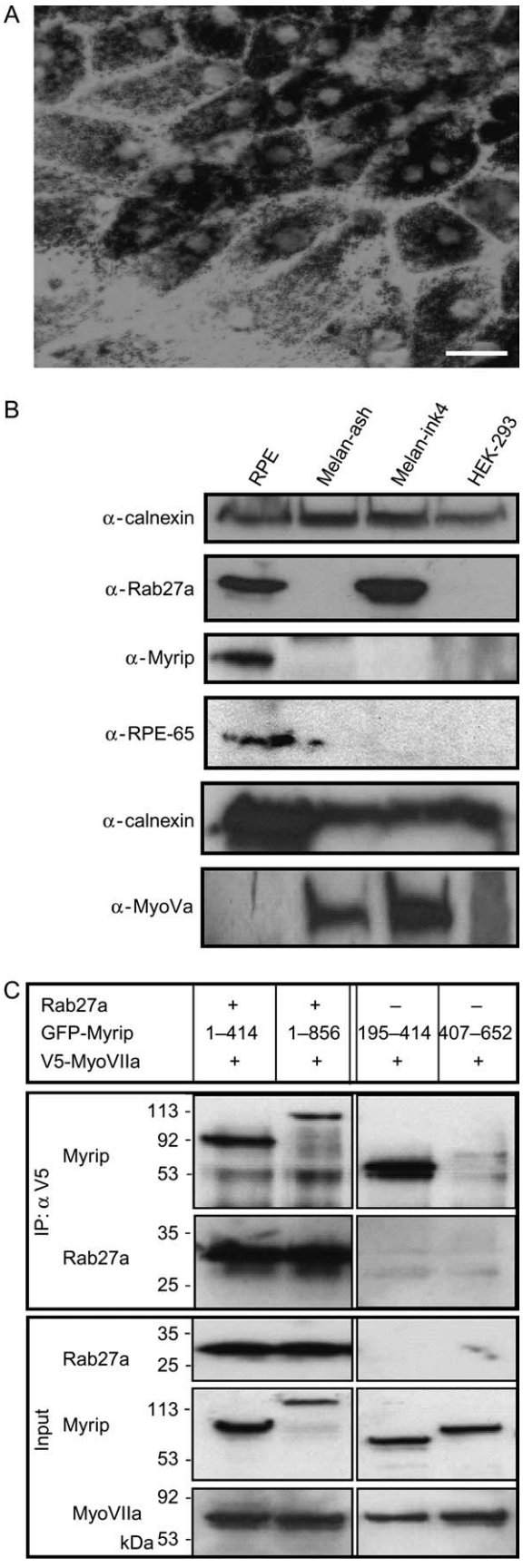

Figure 1: Formation of a Rab27a–Myrip–MyoVIIa tripartite complex. A) Phase contrast image of cultured primary wild-type RPE cells at low magnification (× 40); Bar = 20 μm. B) Protein extracts prepared from wild-type murine RPE primary cells, *ashen* melanocytes, melan-ink (wild type) melanocytes and HEK-293 were separated by SDS–PAGE and immunoblotted for Rab27a, Myrip, RPE65, MyoVa and calnexin (as a loading control) as described under *Materials and Methods*. C) Plasmids encoding V5-MyoVIIa tail, GFP-Myrip and Rab27a were co-transfected into COS-7 cells and the expressed proteins were immunoprecipitated with anti-V5 or anti-Rab27a antibody as described under *Materials and Methods*. The bottom panels show total lysates after transfection, indicating transfection efficiencies. Top panels show immunoprecipitated proteins revealed by the indicated antibodies. [Correction added after publication 3 April 2007: the label in bottom part of Figure 1B was corrected from α-MyoVIIa to α-MyoVa]

We then performed a similar experiment to demonstrate the formation of the complex under more physiological conditions. RPE primary cultures were transduced with adenoviruses (Ad) encoding full-length MyoVIIa fused with GFP. After 2 days, total cell extracts were incubated with anti-GFP antibody and anti-GFP immunoprecipitates were shown to contain Myrip (detected with anti-Myrip antibody) and Rab27a (detected with 4B12 antibody) (unpublished observations). Thus, the heterologous co-immunoprecipitation experiments suggest that a tripartite complex can indeed form, as previously suggested (27).

We then analysed the localization of Myrip and Rab27a in primary cultures of the RPE from adult mice by immunofluorescence microscopy. Rab27a and Myrip were found predominantly on mature melanosomes, regardless of shape or location. Merged images of endogenous Myrip with false-coloured melanosomes revealed the presence of concentric rings surrounding melanosomes (Figure 2 C,D,G,H). The similar pattern of staining suggests that Rab27a and Myrip co-localize in the outer melanosome membrane. It is noteworthy to mention that other non-pigmented structures are also specifically stained with both antibodies, especially in the case of Rab27a (Figure 2I). It is likely that Rab27a and its effectors associate with other cellular organelles, such as secretory granules. Conversely, approximately 20–25% of melanosomes did not exhibit staining (Figure 2J). Melanin is known to quench fluorescence, which may account for some melanized structures without apparent staining.

To confirm the IF studies, we performed immunoelectron microscopy. This high-resolution technique demonstrated that the majority of melanosomes are heavily labelled for Myrip (Figure 2K) and confirmed the co-localization of Myrip and Rab27a on the melanosomal membrane where they were frequently present in clusters (Figure 2L).

Functional requirement of the Rab27a–Myrip–MyoVIIa complex for RPE melanosome motility

The absence of an animal model where Myrip loss-of-function could be studied prompted us to attempt a

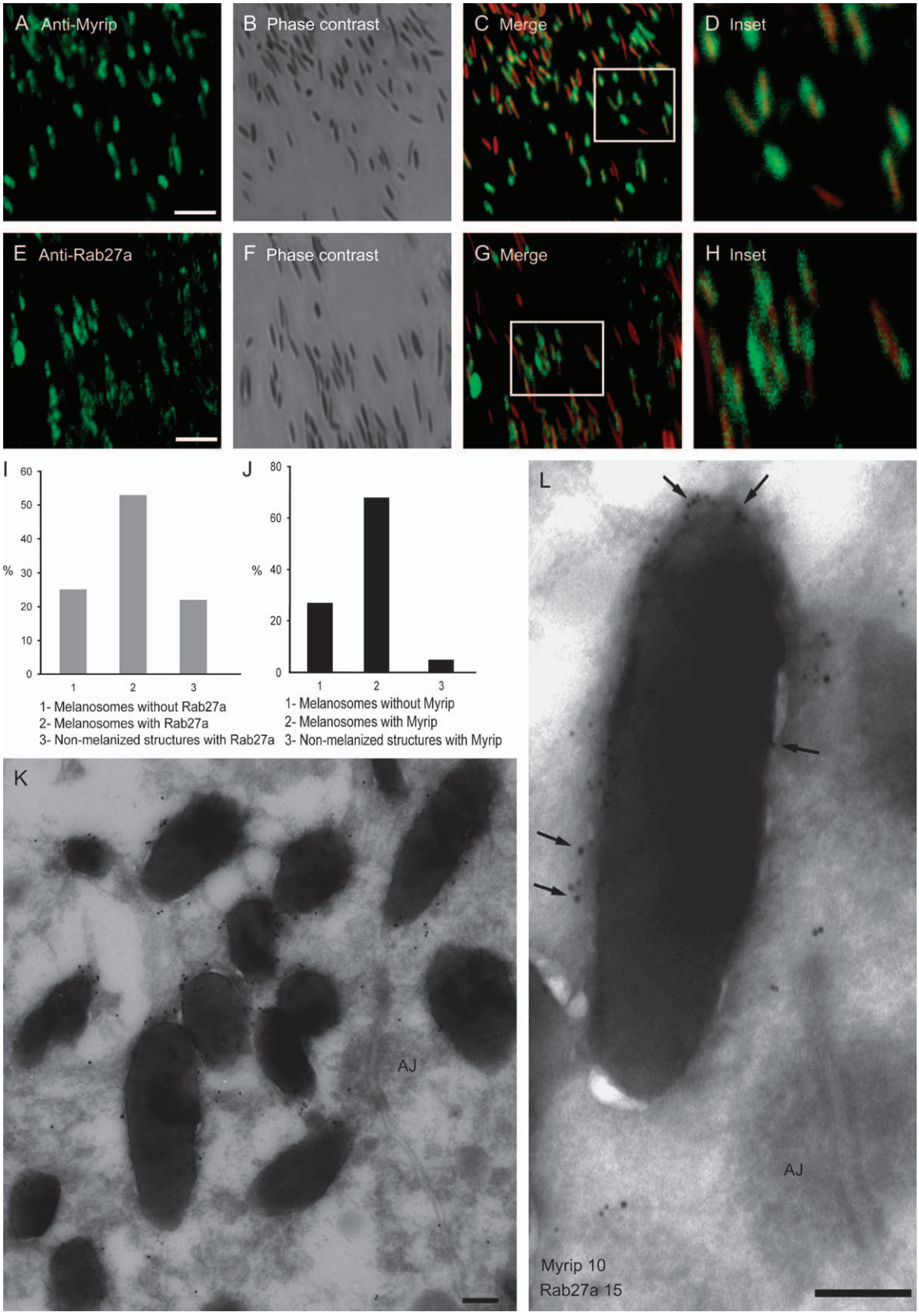

Figure 2: Legend on next page.

short-hairpin RNA (shRNA) approach in cultured RPE primary cells. We designed specific oligonucleotide sequences and tested for their ability to reduce the levels of over-expressed epitope-tagged mouse Myrip in HEK-293 cells (Figure 3A). Out of nine sequences tested, three (shRNA5, 7 and 8) led to a significant decrease in the level of expressed V5-Myrip and were selected for subsequent studies. One of the non-effective shRNA (shRNA4) was also selected to be used as a negative control. The sequences were used to construct adenoviruses expressing these specific shRNAs and the recombinant viruses were used to transduce RPE primary cultures. To confirm the knockdown (KD) of endogenous Myrip in RPE cells, transduced cells were analysed by immunofluorescence (Figure 3B). We confirmed that no apparent Myrip labelling could be detected in cells expressing GFP-shRNA5 (Figure 3B, panel E), -7 and -8 (unpublished observations), as opposed to non-transducing (Figure 3B, panel B) and cells expressing shRNA4 (Figure 3B, panel H). There was no apparent phenotype in any of the mutant or transducing cells, such as changes in cell shape, pigment level or distribution of melanosomes (Figure 3). These observations contrast with the striking clustering of melanosomes in skin melanocytes upon Rab27a/Mlph/MyoVa depletion.

We then studied melanosome dynamics in live RPE-cultured cells using time-lapse microscopy. We analysed *ashen* (Rab27a mutant), *shaker-1* (MyoVIIa mutant) and anti-Myrip shRNA-treated wild-type RPE cells. In order to assess the specificity of the effects, we also performed rescue experiments by reintroducing the missing proteins (in the case of Myrip, an shRNA resistant clone from a different species) using recombinant adenoviruses. Movies depicting melanosome dynamics were obtained for 175 seconds, capturing a frame every 0.5 seconds (see Supplementary Movies) and were analysed using manual-tracking software.

Quantitative analysis of the trajectories of random selected melanosomes revealed significant differences between RPE cultures. Wild-type cells exhibited many motile melanosomes (60.4%, Table 1), undergoing usually short and directional trajectories. In an attempt to determine the cytoskeletal tracts involved, we treated cells with nocodazole (a MT-disrupting agent) and cytochalasin D (which caps actin filaments inducing reorganization of the actin filaments in short actin patches). The efficiency of the treatment was determined by immunofluorescence staining with anti-tubulin and phalloidin, respectively (Figure 4). In nocodazole-treated cells, melanosomes appeared stationary (Tables 1 and 2), while in cytochalasin D-treated cells melanosomes exhibited dynamics similar to those observed in *ashen*, *shaker-1* and Myrip shRNA-treated cells, although generally less pronounced (Tables 1 and 2 and see below). These results implicate both MT- and actin-based motors in the observed melanosome motility.

RPE mutant cells for any of the proposed components of the tripartite complex exhibited more motile melanosomes, which underwent rapid bidirectional movement, including a number of reversal steps (Figure 4; Table 1). Quantitative analysis of our data revealed a 40–60% increase in number of motile melanosomes (typically above 80%) in the absence of Rab27a, Myrip or MyoVIIa, compared to baseline numbers of 50–60% for wild-type cells (Table 1). Cytochalasin D treatment resulted in motility rates between wild type and mutants (Table 1). Consistently, nocodazole-treated cells exhibited less than 20% motile melanosomes (Table 1). The number of reversal steps was also quantified. All three mutant and cytochalasin D-treated cells exhibited a twofold increase in reversal steps when compared to controls (Table 1). The reversal steps are probably the result of the movement along MTs, driven by kinesin and dynein in reverse directions.

It has been previously shown that *shaker-1* RPE primary cultures exhibit an increased average linear displacement profile (5). As confirmed in this study, RPE control cells exhibited several melanosome motility speeds, either stationary or slow movements (typically $\leq$250 nm/second) interrupted by bursts of faster movement (>1000 nm/second) (Figure 4 and Supplementary Movies). Conversely, in mutant RPE cells the bursts of movement were more prolonged and frequent, resulting in a longer average linear displacement (Figure 4; Table 2). When Rab27a or Myrip were deficient, the average linear displacement increased approximately threefold when compared with control values (approximately 30 μm versus 10 μm) (Table 2). In *shaker-1* RPE cells, the increase was less pronounced (approximately 20 μm versus 10 μm). Kymograph profiles of live-cell imaging data show differences in velocity undergone by melanosomes from different mutant backgrounds. In controls, any movement is preceded and followed by an almost absence of movement. In mutant cells, the distance moved in one single step is larger, and melanosomes do not tend to remain stationary following movement (Figure 5). To demonstrate the specificity of the effects, we performed rescue experiments by reintroducing the missing proteins. When transducing adenovirus-encoding GFP-Rab27a, *ashen* cells return to

Figure 2: Subcellular localization of Rab27a and Myrip in RPE. Wild-type murine RPE cells were fixed, permeabilized and labelled with antibodies to Myrip (A) or Rab27a (E), as indicated. B and F) These panels show the corresponding phase contrast images and (C) and (G) are merged fluorescent and phase contrast images. D and H) These panels show boxed regions at higher magnification. Bar = 4 μm. Quantification of melanized and non-melanized structures staining with anti-Rab27a (I) and anti-Myrip (J) are represented. K and L) These panels show immunoelectron microscopy sections of wild-type murine RPE from retinal sections labelled with anti-Myrip antibody and 15 nm protein A–gold (G) or anti-Myrip antibody (10 nm gold) and anti-Rab27a (15 nm gold indicated by arrows) (H). AJ, adherens junction. Bar = 200 nm.

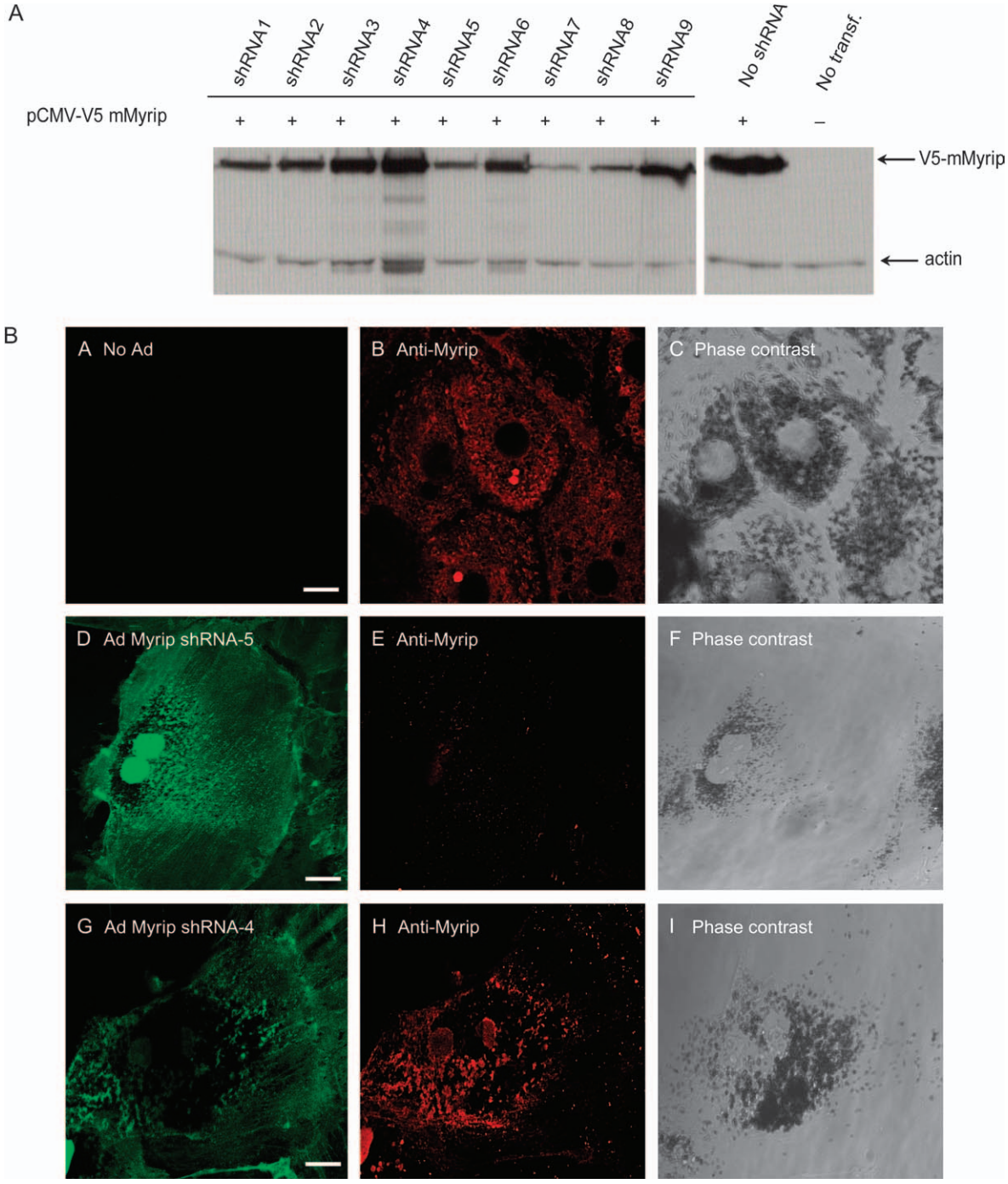

Figure 3: Efficiency of shRNAs to KD Myrip expression. A) HEK-293FT cells were co-transfected with pENTR/CMV-V5-Myrip and pENTR/U6-shRNA. Protein extracts were subjected to immunoblot using anti-V5 antibody. B) Wild-type RPE cells were fixed, permeabilized and subjected to immunofluorescence using anti-Myrip antibody. Wild-type RPE cells expressing no GFP-shRNA (panels A–C), GFP-Myrip shRNA5 (panels D–F) and GFP non-specific shRNA4 (panels G–H) were labelled with Myrip antibody, as indicated. Bar = 20 μm.

control movement kinetics (Tables 1 and 2), as observed above for other parameters. A similar effect was observed with *shaker-1* cells, when GFP-MyoVIIa was introduced (Table 2). As for Myrip, control cells were KD with the relevant shRNA and simultaneously transduced an adeno-virus-encoding rat Myrip, a cDNA resistant to the shRNA effect (unpublished observations). Reintroduction of Myrip restored wild-type melanosome dynamics as shown by all the quantitative methods used (Figure 5; Tables 1 and 2). Also in agreement with the other quantitative analysis,

Table 1: Analysis of motile melanosome population and fraction of reversal steps. Fraction of reversal steps was calculated in a 30-second interval.

RPE source	Percentage of motile melanosomes	Average number of reversal steps
Wild type	60.4 ± 4.3	0.9
Shaker-1	86.2 ± 3.5	1.7
Ashen	87.3 ± 5.2	2.06
Ashen + Ad GFP-Rab27a	56.4 ± 4.1	1
Wild type + Ad GFP-shRNA5 mMyrip	94.1 ± 2.15	2.13
Wild type treated with nocodazole	18.4 ± 5.4	0
Wild type treated with cytochalasin D	72.2 ± 3.6	2.2
Dilute	54.7 ± 1.9	1.1

nocodazole treatment resulted in almost complete melanosome paralysis, while cytochalasin D induced increased average linear displacement comparable to *shaker-1* cells and lower than *ashen* and Myrip shRNA-treated cells (Figure 5; Table 2).

A possible role for MyoVa has been previously proposed, given its reported association with RPE melanosomes (5). Despite our inability to detect MyoVa in RPE cultures by immunoblot, we analysed melanosome dynamics in MyoVa-deficient RPE primary cultures derived from *dilute-lethal* mice. Our analysis revealed motility characteristics similar to wild-type cells (Figure 4; Tables 1 and 2, see also Supplementary Movie 8). Furthermore, we observed that the alterations in melanosome dynamics in Myrip KD RPE cells were not rescued by transduction of Mlph, a Myrip-related protein and the critical linker of Rab27a and MyoVa in skin melanocytes. These results are consistent with normal melanosome distribution in RPE *in vivo* in *dilute* mice (4,5).

Finally, we studied whether there is directionality of melanosome motility in cultured RPE cells. Melanosomes were followed for 30 seconds and the melanosome position relative to the nucleus was calculated for each frame. Our results suggest that melanosomes undergo a directed non-diffusive motion, as expected (unpublished observations). In wild-type and *ashen*-rescued cells, the majority of melanosomes exhibited predominantly motion towards the periphery of the cell (Figure 6A). This centrifugal directionality was disrupted in the Rab27a, Myrip and to a lesser extent MyoVIIa mutant cells and cytochalasin D-treated RPE cells. We also calculated the relative ratio of centrifugal (towards the periphery) and centripetal (towards the nucleus) steps (Figure 6B,C). The histogram in Figure 6B reflects the average velocity obtained for the ratio of anterograde/retrograde steps. Due to a smaller number of reversal steps, control cells have a higher velocity ratio towards the periphery. In the mutant cells analysed, the results suggest lower values and even reversal in directionality in Rab27a- and Myrip-deficient cells (Figure 6B). In the graph depicted in Figure 6C, values >1 demonstrate a centrifugal tendency and <1 a centripetal tendency. The data confirmed that wild-type (and rescued) cells showed a peripheral directionality trend, reflected in the higher number of centrifugal steps while *ashen* and Myrip KD cells exhibited a trend towards reverse directionality (Figure 6). Cytochalasin D-treated and *shaker-1* cells also showed increased number of pauses and reversals but no clear tendency (Figure 6). The milder phenotype observed in *shaker-1* and cytochalasin D-treated RPE cells was consistently observed across the different experiments and analysis methods.

Discussion

The results presented here demonstrate a functional role for the Rab27a–Myrip–MyoVIIa complex in melanosome motility in RPE. We show that the knockout or KD of any of the three proteins elicit the same melanosome dynamics phenotype in primary RPE cultures. Our results confirm previous suggestions that Rab27a is able to associate with different unconventional myosins (such as MyoVa and MyoVIIa) through a pair of related proteins, Mlph and Myrip (11). The evidence presented here also suggests that the Rab27a–Myrip–MyoVIIa complex is involved in anchoring melanosomes to the actin cytoskeleton, which in turn result in directional movement of melanosomes towards the periphery of the cell.

The Rab27a GTPase serves as a maturation sensor that is recruited onto mature secretory granules and lysosome-related organelles (28). Once activated, Rab27a-GTP can potentially interact with at least 11 effector proteins (also called Exophilins). Among these, Myrip (or Slac2-c) and Mlph (or Slac2-a) form a unique family of Rab27- and Myosin-interacting proteins. They can be structurally divided into several domains. At the N-terminus, they contain two sequence homology domains (SHD), SHD1 and SHD2, representing the Rab27-binding domain (29). In the medial region of protein, Mlph contains a complex myosin-binding region, which includes a high-affinity site for a melanocyte-specific isoform of MyoVa (30–32) and a conserved coiled-coil region (33), while the myosin-binding region of Myrip remains less well characterized. Previous studies showed that deletion of the Rab27-binding domain (aa 1–146) did not affect the binding to MyoVIIa (23,24), a finding confirmed in this study. A previous study suggested that the region containing aa 409–602 (24) was necessary for binding to MyoVIIa, a finding not supported by our biochemical data presented in Figure 1. Instead, our data suggest that the myosin-binding region in Myrip maps to aa 195–414. Interestingly, this MyoVIIa-binding region is not conserved between Myrip and Mlph, a finding consistent with the inability of Mlph to bind MyoVIIa (24). We caution however that the interaction

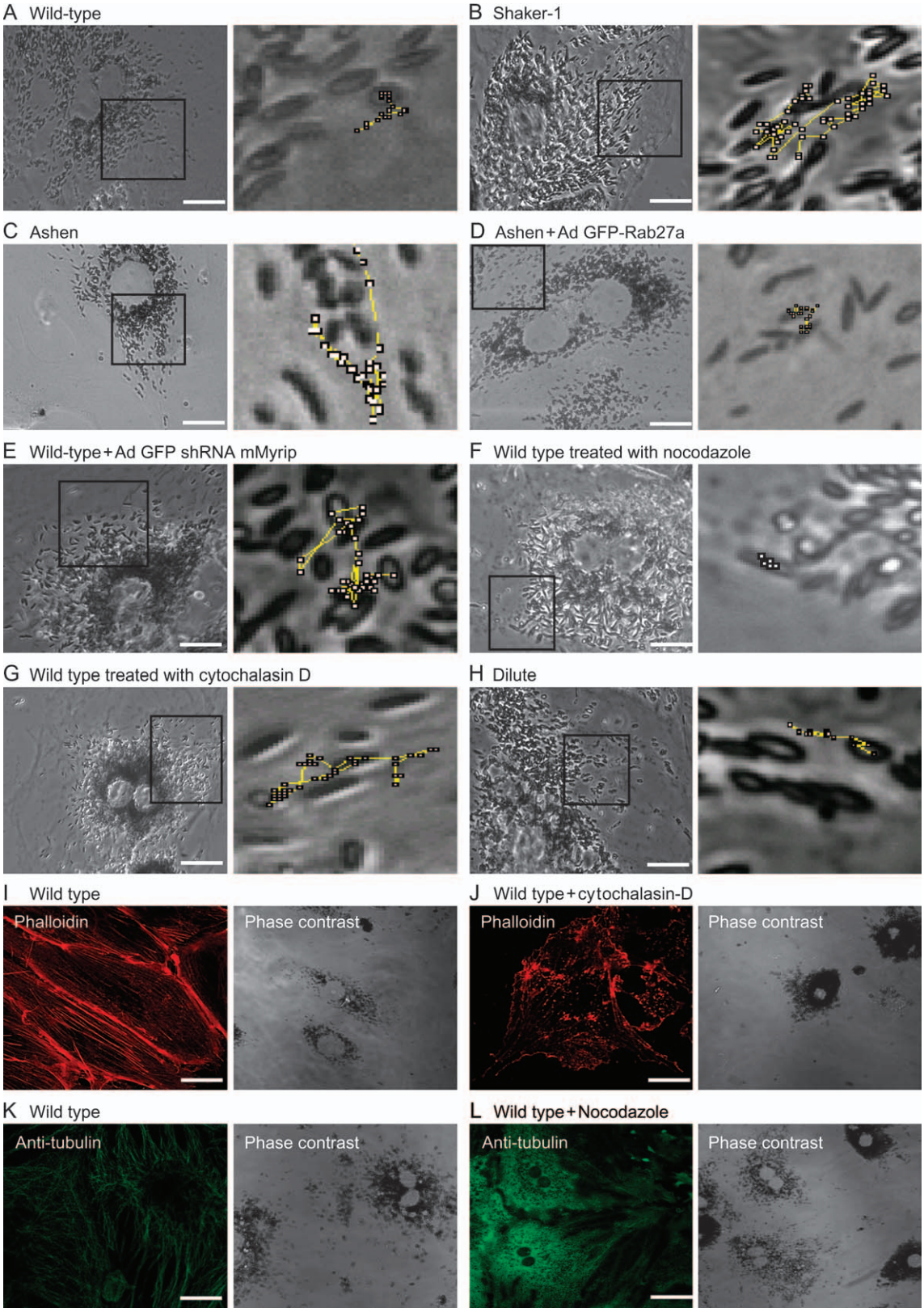

Figure 4: Legend on next page.

Table 2: Mean linear displacement resulting from movements as described under *Materials and Methods* in the indicated RPE cultures (mean ± standard deviation).

RPE source	Melanosome average displacement (μm)
Wild type	9.2 ± 0.4
Wild type + Ad GFP	10.5 ± 0.7
Shaker-1	23.1 ± 1.5
Shaker-1 + Ad GFP-MyoVIIa	10.8 ± 2.3
Ashen	31.8 ± 1.4
Ashen + Ad GFP-Rab27a	10.5 ± 0.6
Wild type + Ad GFP-shRNA5 mMyrip	28.0 ± 1.4
Wild-type + Ad GFP-shRNA7 mMyrip	34.5 ± 2.1
Wild type + Ad GFP-shRNA8 mMyrip	30.5 ± 1.8
Wild type + Ad GFP-shRNA4 mMyrip	10.1 ± 0.7
Wild type + Ad GFP-shRNA5 mMyrip + Ad GFP-rMyrip	9.79 ± 0.8
Wild type treated with nocodazole	2.94 ± 0.9
Wild type treated with cytochalasin D	21.4 ± 1.5
Dilute	14.4 ± 0.8
Wild type + Ad GFP-shRNA5 mMyrip + Ad GFP-mMlph	27.05 ± 2.99

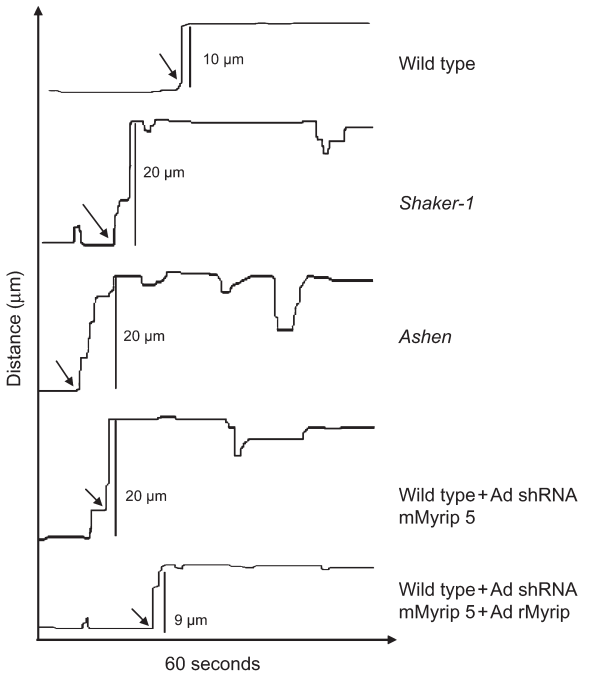

Figure 5: Analysis of melanosome dynamics in RPE primary cultures. Representative kymograph tracings illustrating movement of individual melanosomes are shown for the indicated RPE cultures. Arrows indicate bursts of rapid movement. Tracing was started around 10–15 seconds before rapid movement was noticed.

between Myrip and Myosins may be rather complex, as we have recently observed for Mlph–MyoVa interaction (33). Thus, more detailed studies will be necessary to unravel the molecular basis for these interactions.

MyoVIIa has been previously implicated in melanosome motility in RPE (5,22). Our immunofluorescence and immunoelectron microscopy studies confirmed the RPE melanosomal membrane localization of Rab27a (4) and Myrip (23). Interestingly, we often observed that Myrip-associated gold particles were found in small clusters, suggesting the presence of membrane microdomains, as suggested for Rab27a in secretory granules (34), and Rabs 4, 5, 11 in endosomes (35). The presence of other vesicular structures stained by Myrip and particularly Rab27a raises the possibility that these proteins may serve other roles in membrane-trafficking pathways in RPE cells. Consistently, MyoVIIa has been implicated in lysosomal movement (36) and phagocytosis (37) in the RPE. Additionally, Rab8 was also implicated in actin-dependent movement of melanosomes in skin melanocytes (38) but the relevance of these observations to RPE cells remains unclear.

In intact retinas, the absence of MyoVIIa or Rab27a leads to redistribution of melanosomes from the F-actin-rich apical region and processes to the MT-rich cell body (4,5). The time-lapse microscopy studies and motility analysis described here are broadly consistent with results recently described for the MyoVIIa-deficient RPE cells derived from *shaker-1* mice (5). Furthermore, the new data extend these previous studies in several significant ways. First, we demonstrate that nocodazole treatment lead to an almost complete loss of melanosome movement in mammalian RPE cells. Previous studies in isolated fish RPE cells suggested that MTs and MT-motors were not important for melanosome movements (21). Our studies suggest instead that, at least in mammals, melanosome movements are executed primarily by kinesins and dyneins. Fast-moving melanosomes travel in one direction, pause and often reverse direction (Figures 4; Table 1; Supplementary Movies), as described in melanophores (17,39). Second, our studies clearly implicate Myrip as the

Figure 4: Live-cell imaging of RPE primary cultures and distribution of MTs and actin filaments. Phase contrast images of primary RPE cells at high magnification (× 100) are shown. Zoomed images showing representative trajectories drawn during the entire time frame collected during live-cell imaging illustrates the movement of melanosomes in representative wild-type RPE cell (A), *shaker-1* RPE cell (B), *ashen* RPE cell (C), *ashen* RPE cell transduced with Ad GFP-Rab27a (D), wild-type RPE cell transduced with Ad shRNA5 Myrip (E), wild-type RPE cell treated with nocodazole (F) or cytochalasin D (G) and *dilute* RPE cell (H). Regions used for the movies are marked for each case. Wild-type murine RPE cells were fixed, permeabilized and labelled with phalloidin (I) or anti-tubulin (K), as indicated. Cells treated with 10 μM cytochalasin D were also stained with phalloidin (J), while cells incubated with 10 μM nocodazole were labelled with anti-tubulin (L). Bar = 20 μm.

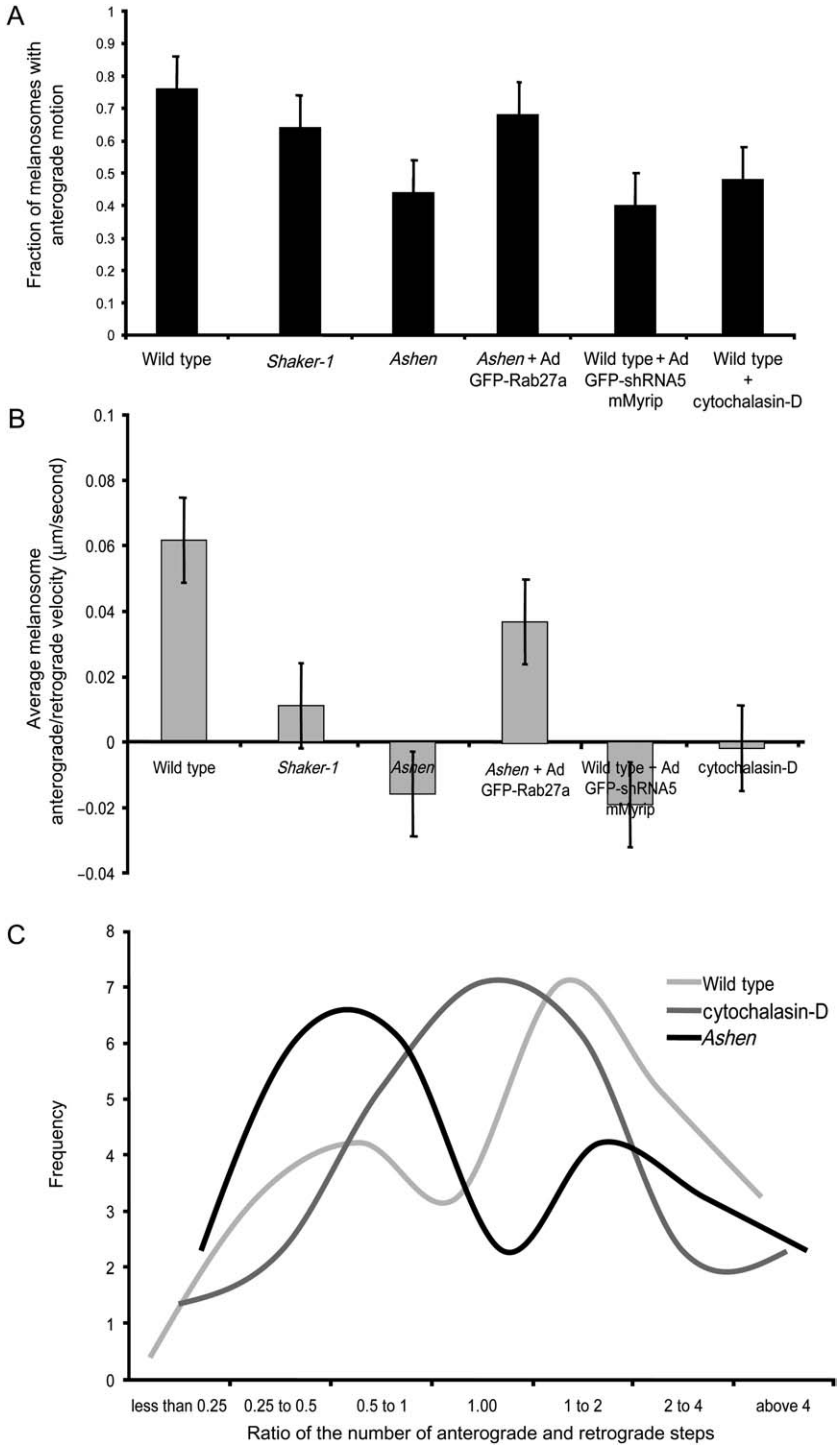

Figure 6: Melanosome motion directionality. Histograms representing the fraction of melanosomes with centrifugal movement (A) and average melanosome anterograde/retrograde velocity (μm/second) (B) are shown for the indicated RPE cultures (mean ± standard deviation). C) Frequency of the ratio of number centrifugal/centripetal steps performed in a population of 25 melanosomes during a 30-second period.

functional linker bridging Rab27a and MyoVIIa because the loss of any one of the three proteins examined resulted in similar phenotypes. We demonstrate that the loss of the Rab27a–Myrip–MyoVIIa complex leads to a significant (50%) increase in the number of motile melanosomes, a greater fluctuation in their orientation and a wider average displacement. Third, our results suggest that melanosomes do move preferentially towards the periphery of the cell in wild-type RPE cells. Furthermore, loss of the Rab27a–Myrip–MyoVIIa complex activity leads to a reversal (or neutrality) in this directionality. This is broadly consistent with extensive observations in skin melanocytes upon loss of Rab27a, Mlph or MyoVa (11). Fourth, melanosome motility in RPE-cultured cells is also affected

by cytochalasin D treatment (Figures 4–6; Tables 1 and 2), whose cells exhibited melanosome dynamics similar to those observed in *ashen*, *shaker-1* and Myrip KD cells. The similarities between cytochalasin D treatment and disruption of any component of the Rab27a–Myrip–MyoVIIa complex suggest that the complex is involved in the tethering of melanosomes with the actin cytoskeleton.

We suggest that loss-of-function of the RPE Rab27a–Myrip–MyoVIIa complex leads to a reduced constraint on MT-based motility, as revealed by the melanosome dynamics alterations described above. Our data imply that this protein complex is involved in the switch from MT- to actin-based motility as proposed in skin melanocytes for the Rab27a–Mlph–MyoVa complex. We also suggest that these data provide further evidence for a tug-of-war mechanism operating between actin and MT transport systems in mammalian RPE cells, as suggested in frog melanophores (17). When the association with actin is disrupted, MT-based movement takes over, and directionality is lost. The association with actin, possibly by disrupting MT minus-end runs of melanosomes, may be responsible for the directionality of movement towards the periphery, which *in vivo* would result in movement into the apical processes, where actin is localized (4). Interestingly, the severity of the phenotypes observed varied, appearing more severe in *ashen* and Myrip KD as compared to *shaker-1* cells. These findings raise the possibility of some functional compensation, namely other possible connections of Rab27a–Myrip with other myosin motor proteins. It is noteworthy that our investigations into a possible role of MyoVa in this process have so far yield only negative data. Furthermore, cytochalasin D-treated cells also showed a milder, intermediate phenotype. The simplest explanation in our view is that the cytochalasin D effect under the conditions used did not completely disrupt all Rab27a–Myrip–MyoVIIa complex activity.

Altogether, our results are consistent with a model whereby MT-based motility is hindered by myosin-driven actin tethering of melanosomes. Nevertheless, the importance of melanosome movements in retinal physiology remains an open question. Mislocalization of melanosomes is not a probable cause for the photoreceptor degeneration found in patients suffering from Usher 1B syndrome caused by MyoVIIa mutations, as this process may be triggered by photoreceptor-specific functions of MyoVIIa and/or a role in RPE phagocytosis leading to a delay in degradation of phagosomes (37). Further work will be needed to clarify these issues.

In summary, mammalian cells seem to have developed a transport unit composed of a small GTPase, linker protein and motor protein enabling dissociation from MT-based motors and connection with the actin cytoskeleton. Using a single membrane marker, the system may use different combinations by varying a small number of linkers and motors.

Materials and Methods

Animals and cell lines

All mice, including *ashen* (C57BL/6J; *ash*/*ash*) (40), *dilute-lethal* (DLS/LeJ) and homozygous agouti *shaker-1* (C57BL/6J; Myo7a$^{4626SB/4626SB}$) (4) colonies were bred and maintained on 12-h light/dark cycle under UK project license PPL 70/6210 at the Central Biomedical Services of Imperial College London. C57BL/6 wild-type mice were purchased from B&K Universal Ltd (Hull, UK).

Retinal pigmented epithelium primary cultures

RPE primary cultures were isolated according to a modified protocol from Wollmann et al. (25,26). Eyes from 3-week-old mice were enucleated, incubated with PBS without Mg^{2+}/Ca^{2+} for 20 min, transferred to warm buffer [PBS plus 1 mM ethylenediaminetetraacetic acid (EDTA)] for 20 min at 37°C, the neuroretina was gently peeled off, and the remaining eyecup was treated with 1 U of preactivated papain (Sigma, Sigma-Aldrich, Gillingham, UK) in dissociation buffer (PBS plus 1 mM EDTA, 26 nM L-cysteine, 1 mg/mL BSA) for 35 min. Papain was activated by incubating 1 U in dissociation buffer for 30 min. Patches of RPE were manually removed with pulses of growth media. Cells were then transferred to media, in order to inactivate the enzyme, centrifuged gently for 5 min at 100 × ***g***, and grown in DMEM high glucose supplemented with 15% FBS, 1× MEM non-essential aa, 100 U/mL penicillin, 100 μg/mL streptomycin, 2.5 μg/mL gentamycin and 50 ng/mL amphothericin B at 37°C and 10% CO_2, for adequate periods of time. Cell cultures reagents were purchased from Gibco unless specified. For experiments involving nocodazole and cytochalasin D, cells were treated with 10 μM of the drug for 1 h at 37°C.

Antibodies

The C-terminal region (aa 644–780) of rat Myrip was fused to glutathione S-transferase as described below and the recombinant protein was produced in *Escherichia coli* and purified on glutathione–Sepharose beads, as described previously (31). Anti-Myrip antibodies were produced in rabbits by Davids Biotechnologie (Regensburg, Germany), affinity purified from sera using the same antigen immobilized on AminoLink Coupling Gel (Pierce, Rockford, IL) as described previously (14,41) and used at 1:20 dilution for immunofluorescence studies, 1:20 for immunoelectron microscopy and 1:250 for immunoblotting. Anti-Rab27a monoclonal 4B12 and polyclonal Q142 antibodies were described previously (14). Anti-MyoVa antibody was raised against exons D and F of mouse MyoVa, affinity purified as described above and used for immunoblot at 1:500. Other antibodies were used as follows: monoclonal anti-RPE65 (Abcam, Cambridge, UK, IF (immunofluorescence): 1:20, IB (immunoblot): 1:250) and polyclonal anti-calnexin (Stressgen, Victoria, Canada, IB: 1:10 000).

Vectors and recombinant viruses

Mouse Myrip cDNA was amplified from pFLCI mMyrip (GenBank acession number AK083225, Fantom clone C630029J04) by polymerase chain reaction (PCR) using Phusion polymerase (New England Biolabs, Hitchin, UK). The PCR fragment was inserted into the pcDNA3.1/V5/His TOPO vector (Invitrogen, Paisley, UK) as instructed by the manufacturer. Full-length Myrip was removed from pcDNA3.1/V5/His using *Hind*III/*Sal*I and inserted into pENTR-GFPC2 using the same restriction sites. Mouse Mlph was excised from pEGFPC2 (33) using *Eco*RI/*Kpn*I and ligated into pENTR-GFPC2 using the same restriction sites. pENTR-GFPC2 and pENTR-GFPC3 were constructed on a backbone of pENTR286 (33), an expression mammalian vector with Gateway® technology (Invitrogen), by swapping part of the promoter and the polylinker with the equivalent sequences containing GFP-coding sequence from pEGFPC2 or pEGFPC3 (Clontech, Mountain View, CA) using *Nde*I/*Bam*HI restriction sites. Rat Myrip was cloned by reverse transcriptase (RT)–PCR using total RNA isolated from rat retina with RNeasy kit (Qiagen, Crawley, UK). RT–PCR was performed according to the manufacturers' instructions using SuperScript II (Invitrogen). The rMyrip-coding sequence was digested with *Eco*RI/*Sal*I and cloned into pENTR-GFPC2 and pENTR-V5C2 using the same restriction sites.

pENTR-V5C2 was also generated based on pENTR286 (33), by swapping part of the promoter and the polylinker with the equivalent sequences containing V5 tag sequence from pCMV-V5 previously generated using *Nde*I/*Bam*HI restriction sites. pCMV-V5 expression mammalian vector was constructed on a backbone of pEGFPC1 (Clontech) by changing GFP for V5 sequence using the *Nhe*I/*Bgl*II restriction sites. In order to generate anti-Myrip antibody, the rMyrip sequence corresponding to aa 644–780 was amplified using pENTR-V5C2 rMyrip as a template. After digestion with *Eco*RI and *Sal*I, the cDNA fragment was cloned into pGEX4T-1 (Amersham, Bucks, UK) using the same restriction sites. Human MyoVIIa head domain (1–632) was cloned by RT–PCR using total RNA isolated from human retina (Eye Bank at Coimbra University Hospital) as described above. Human MyoVIIa tail was subcloned from two EST clones (GenBank acession number BE780659, IMAGE 3872258; GenBank accession number BI835786, IMAGE 5226439). In order to clone full-length hMyoVIIa-coding sequence into the mammalian expression vector pENTR286 with Gateway technology (33), a *Bsi*WI and a *Spe*I restriction sites were inserted by PCR. The order of the cloning was as follows: MyoVIIa tail (aa 1111 stop) using *Spe*I/*Not*I, MyoVIIa tail (aa 633–1110) using *Bsi*WI/*Spe*I and MyoVIIa head (aa 1–632) using *Eco*RI/*Bsi*WI. In order to tag MyoVIIa with GFP at the N-terminus, GFP was removed from pcDNA3.1/V5/His GFP using *Eco*RI/*Eco*RI and inserted into pENTR286 MyoVIIa full length using the *Eco*RI restriction site. pcDNA3.1/V5/His GFP was previous generated by amplification of GFP with pEGFPC1 (Clontech) as a template and cloned into pcDNA3.1/V5/His TOPO (Invitrogen) according to the manufacturers' instructions. In order to generate Ad GFP-Rab27a, the mammalian expression cassette (CMV promoter/GFP/rRab27a/polyA) was amplified from pEGFP-rRab27a using Phusion, cut with *Sal*I/*BamH*I and cloned into pENTR286 (33) using the same restriction sites. Short-hairpin RNA (shRNA) -expressing vectors were constructed by inserting an inverted repeat of Myrip-specific 21-nucleotide sequences into pENTR/U6 plasmid harbouring PolIII U6 promoter obtained from Invitrogen. For shRNA targeting of mouse Myrip, the oligonucleotides were annealed and ligated into pENTR/U6 according to manufacturers' instructions (underline indicates RNA interference target sequences). The following oligonucleotides were used: shRNA mMyrip 5 sense: CACCGCAGAGAGACTTCAATCTTCGCGAACGAAGATTGAAGTCTCTCTGC, antisense: AAAAGCAGAGAGACTTCAATCTTCGTTCGCGAAGATTGAAGTCTCTCTGC; shRNA mMyrip 7 sense: CACCGGAGGATTGTTTGAACCAAACTTCAAGAGAGTTTGGTTCAAACAATCCTCC, antisense: AAAAGGAGGATTGTTTGAACCAAACTCTCTTGAAGTTTGGTTCAAACAATCCTCC; shRNA mMyrip 8 sense: CACCGCTGAGAAATAGACTGTATGATTCAAGAGATCATACAGTCTATTTCTCAGC, antisense: AAAAGCTGAGAAATAGACTGTATGATCTCTTGAATCATACAGTCTATTTCTCAGC and shRNA mMyrip 4 sense: CACCGGACTTGATGGAGCCTGATCTTTCAAGAGAAGATCAGGCTCCATCAAGTCC. All plasmids were verified by DNA sequencing. Myrip shRNA or cDNA encoding the proteins of interest were cloned according to manufacturers' instructions into pAd adenoviral vector from Invitrogen using Gateway technology.

Cell culture

Melan-ink4a melanocytes were maintained in RPMI-1640 supplemented with 10% FCS, 200 nM phorbol 12-myristate 13-acetate and 200 pM cholera toxin at 37°C with 10% CO_2, as described previously (33). 293FT human embryo kidney cells obtained from Invitrogen were grown in DMEM in the presence of 10% FBS and antibiotics at 37°C and 10% CO_2. Cells were co-transfected in six-well plates with pENTR/U6-Myrip shRNA and pENTR-V5-mMyrip using Lipofectamine (Invitrogen) as instructed by the manufacturer. At 24 h post-transfection cells were lysed in plates by using lysis buffer [50 mM Tris–HCl (pH 7.4), 150 mM NaCl, 1% CHAPS {3-[(3-Cholamidopropyl)dimethylammonio]-1-propanesulfonate}, 1 mM phenylmethylsulphonyl fluoride (PMSF), 1 mM DTT and complete protease inhibitor cocktail (Roche, West Sussex, UK)]. Proteins were separated by SDS–PAGE and visualized by immunoblotting using PVDF (polyvinylidene difluoride) membranes and anti-V5 antibody (Invitrogen) (1:2000). In order to produce adenoviral particles, 293A cells obtained from Invitrogen were grown in DMEM containing 10% FBS, 1× non-essential aa, 100 U/mL penicillin and 100 μg/mL streptomycin at 37°C and 10% CO_2. Cells were transfected in 60-mm culture dishes with pAd DNA previously digested with *Pac*I using Lipofectamine 2000 (Invitrogen) as instructed by the manufacturer. Medium containing adenovirus particles was collected when approximately 80% cytopathic effect is observed (typically 10–13 days post-transfection) and centrifuged as described by Invitrogen. Adenovirus expressing shRNA under the control of the PolIII promoter and the GFP gene under the control of CMV promoter or GFP-Rab27a, GFP-rMyrip, GFP-hMyoVIIa genes also under the control of the cytomegalovirus promoter were used in the range 1×10^7–1×10^8 particles per millilitre to transduce RPE primary cultures from *ashen*, *shaker-1* and wild-type mice.

Immunoprecipitation

Cells grown in 60-mm culture dishes were lysed for 30 min in lysis buffer [50 mM Tris–HCl (pH 7.4), 150 mM NaCl, 1% CHAPS, 1 mM PMSF, 1 mM DTT and complete protease inhibitor cocktail (Roche)]. Lysates were clarified by microcentrifugation for 15 min at 13000 × ***g*** at 4°C. For V5 immunoprecipitations, lysates diluted 2 times with the same buffer without detergents were incubated with 2 μg of V5 antibody overnight at 4°C with rotation, and immune complexes were captured also overnight at 4°C of incubation with 50 μL of protein G–Sepharose beads (Amersham). Immune complexes were washed with lysis buffer and incubated in SDS gel-loading buffer for 3 min at 95°C. Proteins were separated by SDS–PAGE and visualized by immunoblotting as above. The same basic protocol was used with RPE cells, with the exception that immunoprecipitation was performed with 2 μg of GFP antibody (Abcam) and complexes were captured with protein A–Sepharose beads (Amersham).

Immunofluorescence and confocal microscopy

Cells used for immunofluorescence were grown on glass coverslips, and transducing adenovirus where indicated. Cells were washed with PBS, fixed with 4% (w/v) paraformaldehyde (PFA) in PBS for 15 min, rinsed twice with PBS, incubated for 10 min with 50 mM NH_4Cl in PBS and permeabilized with 0.05% saponin/0.5% BSA in PBS for 45 min. Permeabilized cells were incubated with the primary antibodies for 1 h at room temperature, followed by four washes and incubation with Alexa 568-conjugated and Alexa 488-conjugated secondary antibodies (Molecular Probes, Paisley, UK, 1:200) for another hour at room temperature. All incubations and washing steps were carried out in 0.05% saponin/0.5% BSA in PBS. The coverslips were mounted in ImmunoFluor medium (ICN, Basingstone, Hants, UK) and visualized using a Leica DM-IRBE confocal microscope (Leica, Wetzlar, Germany). Images were processed using TCS-NT software (Leica) and ADOBE PHOTOSHOP 5.5 software. All images shown are single sections in the *z*-plane and representative of at least 80% of transducing cells.

Time-lapse analysis of melanosome dynamics and quantitative analysis

Living cells were visualized in a time-lapse bright field microscope (Zeiss Axiovert, UK), using a × 100 oil objective. The temperature of the chamber was maintained at 37°C, using a hot air source. Groups of 350 images were acquired at 500-millisecond intervals, totalizing 175 seconds, with a CCD camera (Hamamatsu Orca, ER, Shizuoka-Ken, Japan). Image acquisition was performed using OPENLAB 5.0 software. Image stacks obtained were then imported into IMAGEJ software (National Institutes of Health, Bethesda, MA, USA) and linear displacement in two dimensions and average velocity were measured using the Manual-Tracking plugin (http://rsb.info.nih.gov/ij/plugins). A total of 100 motile melanosomes were sampled randomly from three independent cultures of primary RPE cells for each mutant and controls. Kymographs were generated using the Multiple Kymograph plugin (http://rsb.info.nih.gov/ij/plugins). The percentage of motile melanosomes was done by randomly tracking melanosomes and considering as immotile melanosomes those moving less than 1 μm during the time frame analysed (175 seconds) ($n > 400$ for each case). The total number of reversals steps was calculated in 25 moving melanosomes during a period of 30 seconds, and defined as a movement in the opposite direction the melanosome followed previously. Directionality analysis was performed for some of the cultured RPE cells. Melanosomes were followed during 30 seconds and

their *x* and *y* co-ordinates recorded. Position of the melanosome relative to the nucleus was calculated for each frame. A positive value was considered centrifugal movement and a negative value as centripetal movement.

Electron microscopy

Mouse eyes were fixed in 4% PFA, 0.1% glutaraldehyde in 0.1 M phosphate buffer and embedded as previously described (4). Sections (70 nm) were cut at −120°C, picked up in 1:1 sucrose:methylcellulose and immunogold labelled as described (4). For labelling with rabbit primary antibodies, swine anti-rabbit IgG intermediate antibody was used before protein A–gold to enhance the signal. For Myrip and Rab27a double labelling, sections were first labelled with anti-Myrip, intermediate antibody and 10 nm protein A–gold, were then fixed in 1% glutaraldehyde for 15 min and finally were labelled with anti-Rab27a, intermediate antibody and 15 nm protein A–gold. Sections were viewed under a Joel 1010 electron microscope.

Acknowledgments

The authors would like to thank Tanya Tolmachova, Holly Graham and Emilie Mules for mouse breeding and Alistair Hume for preparing the anti-MyoVa antibody. This work was supported by the Wellcome Trust and the BBSRC (Biotechnology and Biological Sciences Research Council) (to M. C. S.), by the Deutsche Forschungsgemeinschaft grants DFG STR480/8-2 and STR480/9-1 (to O. S.) and by a PhD studentship from Foundation for Science and Technology, Portugal (to V. S. L.).

Supplementary Material

Time-lapse movies showing melanosome dynamics in RPE primary cultured cells. Images were captured every 0.5 seconds, and the movies show one in each two frames, at a frame rate of 7 fps. Movie 1: wild-type RPE cell; Movie 2: *shaker-1* RPE cell; Movie 3: *ashen* RPE cell; Movie 4: *ashen* RPE cell transduced with Ad GFP-Rab27a; Movie 5: Wild-type RPE cell transduced with Ad shRNA5 Myrip; Movie 6: wild-type RPE cell treated with nocodazole; Movie 7: wild-type RPE cell treated with cytochalasin D; Movie 8: *dilute* RPE cell.

Supplemental materials are available as part of the online article at http://www.blackwell-synergy.com

References

1. Futter CE. The molecular regulation of organelle transport in mammalian retinal pigment epithelial cells. Pigment Cell Res 2006;19: 104–111.
2. Strauss O. The retinal pigment epithelium in visual function. Physiol Rev 2005;85:845–881.
3. Jeffery G. The albino retina: an abnormality that provides insight into normal retinal development. Trends Neurosci 1997;20:165–169.
4. Futter CE, Ramalho JS, Jaissle GB, Seeliger MW, Seabra MC. The role of Rab27a in the regulation of melanosome distribution within retinal pigment epithelial cells. Mol Biol Cell 2004;15:2264–2275.
5. Gibbs D, Azarian SM, Lillo C, Kitamoto J, Klomp AE, Steel KP, Libby RT, Williams DS et al. Role of myosin VIIa and Rab27a in the motility and localization of RPE melanosomes. J Cell Sci 2004;117: 6473–6483.
6. Marks MS, Seabra MC. The melanosome: membrane dynamics in black and white. Nat Rev Mol Cell Biol 2001;2:738–748.
7. Wu X, Hammer JA III. Making sense of melanosome dynamics in mouse melanocytes. Pigment Cell Res 2000;13:241–247.
8. Wu X, Bowers B, Rao K, Wei Q, Hammer JA III. Visualization of melanosome dynamics within wild-type and dilute melanocytes suggests a paradigm for myosin V function In vivo. J Cell Biol 1998;143: 1899–1918.
9. Van Den Bossche K, Naeyaert JM, Lambert J. The quest for the mechanism of melanin transfer. Traffic 2006;7:769–778.
10. Fukuda M. Versatile role of Rab27 in membrane trafficking: focus on the Rab27 effector families. J Biochem (Tokyo) 2005;137:9–16.
11. Seabra MC, Coudrier E. Rab GTPases and myosin motors in organelle motility. Traffic 2004;5:393–399.
12. Stinchcombe J, Bossi G, Griffiths GM. Linking albinism and immunity: the secrets of secretory lysosomes. Science 2004;305:55–59.
13. Wu X, Rao K, Bowers MB, Copeland NG, Jenkins NA, Hammer JA III. Rab27a enables myosin Va-dependent melanosome capture by recruiting the myosin to the organelle. J Cell Sci 2001;114:1091–1100.
14. Hume AN, Collinson LM, Hopkins CR, Strom M, Barral DC, Bossi G, Griffiths GM, Seabra MC et al. The leaden gene product is required with Rab27a to recruit myosin Va to melanosomes in melanocytes. Traffic 2002;3:193–202.
15. Provance DW, James TL, Mercer JA. Melanophilin, the product of the leaden locus, is required for targeting of myosin-Va to melanosomes. Traffic 2002;3:124–132.
16. Nascimento AA, Roland JT, Gelfand VI. Pigment cells: a model for the study of organelle transport. Annu Rev Cell Dev Biol 2003;19:469–491.
17. Gross SP, Tuma MC, Deacon SW, Serpinskaya AS, Reilein AR, Gelfand VI. Interactions and regulation of molecular motors in Xenopus melanophores. J Cell Biol 2002;156:855–865.
18. Kural C, Kim H, Syed S, Goshima G, Gelfand VI, Selvin PR. Kinesin and dynein move a peroxisome in vivo: a tug-of-war or coordinated movement? Science 2005;308:1469–1472.
19. Tabb JS, Molyneaux BJ, Cohen DL, Kuznetsov SA, Langford GM. Transport of ER vesicles on actin filaments in neurons by myosin V. J Cell Sci 1998;111:3221–3234.
20. Bridgman PC. Myosin Va movements in normal and dilute-lethal axons provide support for a dual filament motor complex. J Cell Biol 1999;146: 1045–1060.
21. King-Smith C, Paz P, Lee CW, Lam W, Burnside B. Bidirectional pigment granule migration in isolated retinal pigment epithelial cells requires actin but not microtubules. Cell Motil Cytoskeleton 1997; 38:229–249.
22. Liu X, Ondek B, Williams DS. Mutant myosin VIIa causes defective melanosome distribution in the RPE of shaker-1 mice. Nat Genet 1998;19:117–118.
23. El-Amraoui A, Schonn JS, Kussel-Andermann P, Blanchard S, Desnos C, Henry JP, Wolfrum U, Darchen F, Petit C et al. MyRIP, a novel Rab effector, enables myosin VIIa recruitment to retinal melanosomes. EMBO Rep 2002;3:463–470.
24. Fukuda M, Kuroda TS. Slac2-c (synaptotagmin-like protein homologue lacking C2 domains-c), a novel linker protein that interacts with Rab27, myosin Va/VIIa, and actin. J Biol Chem 2002;277: 43096–43103.
25. Edwards RB. Culture of rat retinal pigment epithelium. In Vitro 1977;13:301–334.
26. Wollmann G, Lenzner S, Berger W, Rosenthal R, Karl MO, Strauss O. Voltage-dependent ion channels in the mouse RPE: comparison with Norrie disease mice. Vision Res 2006;46:688–698.
27. Kuroda TS, Fukuda M. Functional analysis of Slac2-c/MyRIP as a linker protein between melanosomes and myosin VIIa. J Biol Chem 2005; 280:28015–28022.
28. Seabra MC, Wasmeier C. Controlling the location and activation of Rab GTPases. Curr Opin Cell Biol 2004;16:451–457.

29. Kuroda TS, Fukuda M, Ariga H, Mikoshiba K. The Slp homology domain of synaptotagmin-like proteins 1-4 and Slac2 functions as a novel Rab27A binding domain. J Biol Chem 2002;277:9212–9218.
30. Li XD, Jung HS, Mabuchi K, Craig R, Ikebe M. The globular tail domain of myosin Va functions as an inhibitor of the myosin Va motor. J Biol Chem 2006;281:21789–21798.
31. Strom M, Hume AN, Tarafder AK, Barkagianni E, Seabra MC. A family of Rab27-binding proteins. Melanophilin links Rab27a and myosin Va function in melanosome transport. J Biol Chem 2002;277: 25423–25430.
32. Wu X, Wang F, Rao K, Sellers JR, Hammer JA III. Rab27a is an essential component of melanosome receptor for myosin Va. Mol Biol Cell 2002;13:1735–1749.
33. Hume AN, Tarafder AK, Ramalho JS, Sviderskaya EV, Seabra MC. A coiled-coil domain of melanophilin is essential for myosin Va recruitment and melanosome transport in melanocytes. Mol Biol Cell 2006;17:4720–4735.
34. Desnos C, Schonn JS, Huet S, Tran VS, El-Amraoui A, Raposo G, Fanget I, Chapuis C, Menasche G, de Saint Basile G, Petit C, Cribier S, Henry JP, Darchen F et al. Rab27A and its effector MyRIP link secretory granules to F-actin and control their motion towards release sites. J Cell Biol 2003;163:559–570.
35. Sonnichsen B, De Renzis S, Nielsen E, Rietdorf J, Zerial M. Distinct membrane domains on endosomes in the recycling pathway visualized by multicolor imaging of Rab4, Rab5, and Rab11. J Cell Biol 2000; 149:901–914.
36. Soni LE, Warren CM, Bucci C, Orten DJ, Hasson T. The unconventional myosin-VIIa associates with lysosomes. Cell Motil Cytoskeleton 2005; 62:13–26.
37. Gibbs D, Kitamoto J, Williams DS. Abnormal phagocytosis by retinal pigmented epithelium that lacks myosin VIIa, the Usher syndrome 1B protein. Proc Natl Acad Sci U S A 2003;100:6481–6486.
38. Chabrillat ML, Wilhelm C, Wasmeier C, Sviderskaya EV, Louvard D, Coudrier E. Rab8 regulates the actin-based movement of melanosomes. Mol Biol Cell 2005;16:1640–1650.
39. Gross SP, Welte MA, Block SM, Wieschaus EF. Coordination of opposite-polarity microtubule motors. J Cell Biol 2002;156: 715–724.
40. Barral DC, Ramalho JS, Anders R, Hume AN, Knapton HJ, Tolmachova T, Collison LM, Goulding D, Authi KS, Seabra MC et al. Functional redundancy of Rab27 proteins and the pathogenesis of Griscelli syndrome. J Clin Invest 2002;110:247–257.
41. Seabra MC, Ho YK, Anant JS. Deficient geranylgeranylation of Ram/Rab27 in choroideremia. J Biol Chem 1995;270:24420–24427.